Vol. 48, No. 2 (2026) 222-236, DOI: 10.24874/ti.1958.06.25.11

Tribology in Industry

www.tribology.rs

RESEARCH

Effect of GnPs on Erosion Wear of BFRP Composite Pipes Under High Temperature Conditions

Mehmet Bagci[a,*], Musa Demirci[b], Seyit Mehmet Demet[a], Harun Sepetcioglu[c]

[a]*Mechanical Engineering Department, Eng. and Nat. Sci. Fac., Konya Technical University, Konya 42250, Turkey,*
[b]*Mechanical Engineering Department, Eng. and Nat. Sci. Fac., KTO Karatay University, Konya 42020, Turkey,*
[c]*Department of Metallurgy and Materials Eng., Faculty of Technology, Selcuk University, Konya 42250, Turkey.*

Keywords:

Solid particle erosion
Basalt fiber pipes
Graphene nanoplatelets (GnPs)
High temperature
Impingement angle
Wear resistance

* Corresponding author:

Mehmet Bagci
E-mail: mbagci@ktun.edu.tr

Received: 10 June 2025
Revised: 28 July 2025
Accepted: 10 November 2025

A B S T R A C T

Basalt fiber reinforced polymer (BFRP) composite pipes were reinforced with 0.25 wt% graphene nanoplatelets by ultrasonic mixing technique. Solid particle erosion tests were carried out at 23 °C, 50 °C and 100 °C and different impingement angles (30°, 60°, 90°). The highest erosion rate in Basalt pipe was at 90° erosive particle impingement angles, while in graphene nanoplate reinforced pipes, this rate was realized at 60° and 90°. In other words, at 23°C, the erosion resistance gain achieved with graphene addition was 1,52-2,89 times greater depending on the impact angle, but even experiments conducted at 50°C and 100°C demonstrated a 55% increase in the practical relevance of graphene use. To provide evidence for damage mechanisms based on the detailed data obtained, the focus was on clearly demonstrating the quantitative impact of graphene's presence using scanning electron microscopy. Furthermore, enhanced performance and durability of additive composite materials will pave the way for their widespread use in industrial applications, with sectoral output.

1. INTRODUCTION

Composites that have a dominant role in study are increasingly gaining popularity as an alternative to traditional glass and carbon fiber-reinforced composites due to their advantages such as high mechanical strength, low weight, corrosion resistance, and environmental sustainability [1]. Furthermore, their tubular form has made them a significant choice in the construction industry, particularly in bridges, viaducts, and building columns. They are increasingly used as structural support elements in infrastructure systems, in water and wastewater transportation systems due to their corrosion resistance; in the oil and gas industry, in oil drilling pipes and platforms due to their chemical resistance; in the energy sector, in wind turbines and power transmission line poles due to their lightness and durability; and in the transportation sector, in ship, aircraft, and train components [2,3]. However, the long-term performance of BFRP composites in harsh environmental conditions remains a subject of

research. Especially, wear of industrial and agriculturally based components is currently one of the most serious issues. Therefore, the current research reports on the influence of nanotubes (NTs) loading on the three-body abrasive behavior of bidirectional silk fibre (SF) and basalt fibre (BF) reinforced epoxy (Ep) composites. Wear resistance and overall durability are critical concerns in applications such as aerospace, automotive, marine and civil infrastructure, where they are exposed to high temperatures, mechanical stresses and abrasive wear [4]. To overcome the challenges inherent in erosive wear, studies on incorporating nanofillers such as graphene nanoplatelets (GnPs) into the polymer matrix to improve the mechanical and tribological properties of BFRP composites will be significant. Furthermore, carbon nanotubes (CNTs) subjected to specific treatments have been found to significantly reduce the coefficient of friction and wear volume loss in basalt/epoxy composites, leading to significant improvements in dynamic mechanical and thermal properties. Such modifications could contribute to providing more reliable and cost-effective solutions by extending the industrial service life of BFRP composites [5].

Graphene is of great interest in the field of composite materials due to its exceptional mechanical strength, thermal conductivity, and self-lubricating properties. When incorporated into polymer matrices, graphene has been shown to improve interfacial adhesion, reduce water absorption, and increase wear resistance, making it an ideal candidate for reinforcing BFRP composites [6,7]. The addition of graphene to BFRP composites significantly improves the mechanical, thermal and electrical performance of the material. It increases the strength of the polymer matrix, increasing tensile and compressive strengths, making it harder for microcracks to spread, improving fatigue performance, and increasing the impact strength of the composite, making it more resistant to sudden loads and shocks [8]. In addition, due to the high thermal conductivity of graphene, the thermal dissipation capacity of the composite is increased, reducing thermal stress and making the material more stable under extreme temperature conditions [9-11].

In glass fiber reinforced epoxy composites, by adding 0.5-1% by weight graphene nano-plates, a 36.74% improvement in the friction coefficient and a 28.47% improvement in the wear rate were achieved, and in this context, the effects of load and sliding distance on tribological behavior were analyzed in detail [12]. In addition, studies on natural fiber composites also reveal important results. It has been observed that the addition of nano graphene to hybrid jute-basalt composites significantly improves tribological properties. When 0.2 wt% graphene is added to hybrid composites, the friction coefficient and specific wear rate in contact with the jute surface are 28.95%; and with the addition of 0.4 wt% graphene on the basalt surface, this improvement is 53%. In addition, in the wear tests conducted at 650rpm and 850rpm speeds of the pin on disk in hybrid composites containing 0.6 wt% graphene, increases of 26.36% and 24.66% in specific wear rate are reported, respectively [13].

Due to its renewability, research on the effects of biomaterials in composites is also important for the advancement of engineering materials. Basalt fiber has been used as a filler material to increase its fatigue life. These processes, in addition to tensile testing, have also contributed to significant improvements in the fatigue life of basalt fiber [14]. The addition of graphene nanoplatelets (GnPs) to CFRP composite pipe also increases the wear resistance of the composite [15]. This feature allows pipes to have a longer life in applications where they are subject to friction (e.g. due to liquids or solid particles passing through the pipe). Recent studies have shown that the addition of graphene nanoplatelets (GnPs) can significantly reduce the negative effects of hydrothermal aging, mechanical loading and abrasive wear, thus extending the service life of composite pipes in industrial applications [16]. As a result, the addition of graphene nanoplatelets to BFRP composite pipes improves many properties of the composite, such as mechanical, thermal, corrosion and impact resistance, allowing the pipes to have a wider range of uses and to perform better in harsh environmental conditions [17].

The wear behavior of BFRP composites is a critical factor in determining their suitability for applications involving sliding wear or erosive wear. Many studies investigating the tribological properties of graphene-reinforced composites have shown that GnPs can act as a solid lubricant

and reduce friction coefficients and wear rates by forming a stable transfer film at the interface between sliding surfaces. For example, the study found that the addition of surface-modified GnPs to basalt fiber-reinforced epoxy composites increased wear resistance by up to 100% under varying load conditions, with optimum performance being achieved at a GnP concentration of 0.3 wt% [18]. Similarly, another work reported that uniform coating of graphene on basalt fibers increased the interfacial adhesion between the fibers and the polymer matrix, leading to significant improvements in tensile strength, flexural strength, and wear resistance [19]. Despite these developments, the effect of GnPs on the wear behavior of BFRP composite pipes under high-temperature conditions has not been sufficiently investigated. High temperatures can exacerbate the degradation of polymer matrices, leading to increased wear rates and decreased mechanical performance. Understanding the interaction between graphene reinforcement, temperature, and wear mechanisms is essential to optimize the design and performance of BFRP composites in high-temperature applications. Recent studies have shown that GnPs can increase the thermal stability and mechanical stiffness of basalt fiber composites, making them suitable for use in high-temperature environments [20,21].

The novelty of the work focused on the particle impact behavior of BFRP composite pipes, which offer a combination of strength and lightness, and whose use in heat transfer lines, where heat efficiency is a significant factor, is particularly questionable. Furthermore, the current research study examined the erosion wear properties and wear damage mechanisms of graphene nanoplate additives (GnPs) to be incorporated into BFRP composite materials. This study emphasizes the differences in wear resistance due to surface variations in temperature environments (50°C and 100°C), where the thermal efficiency of graphene is primarily questioned. Prioritizing the transfer of the experimental results to industry, the study accelerated studies to directly contribute to the adaptation of performance and lifespan improvements in composite materials used in pipe transfer lines carrying hot components to alternative sectors, and the field application phase has begun.

2. TEST METHODOLOGY

2.1 Materials, pipe dimensions and preparation

Composite pipes were produced using the filament winding technique, which involved both unreinforced and graphene nanoplatelets (GnPs) reinforced Basalt Fiber Reinforced Polymer (BFRP) specimens. The pipes had an outer diameter of 76 mm, a wall thickness of 1.95 mm, and a total length of 1 m. Monofilament basalt fibers (400 tex, diameter of 13 μm) were utilized as the reinforcement, and these were supplied by Kamenny Vek, Inc., Dubna, Russian Federation. The epoxy matrix system consisted of EPIKOTE™ 828 LVEL as the resin and EPIKURE™ 866 as the hardener, both sourced from Hexion, Inc., Columbus, Ohio, USA. The properties of the epoxy resin and basalt fibers are presented in Table 1.

Table 1. Material properties of the epoxy system and basalt fibers.

Type	E GPa	σ MPa	ε mm/mm	ρ g/cm^3
Basalt fiber	90–95	2900–3200	–	2.48
Epoxy resin	3.2	70–75	4–5	1.25

For nano-reinforcement, non-functionalized graphene nanoplatelets (GnPs - the optimal GnP content was determined as 0.25 wt%) with a surface area of 800 g/m^2, layer thicknesses of 3–7 nm, and an average width of 1.5 μm (Nanografi Nano Technology) were incorporated into the matrix. The preparation process involved first dispersing the GnPs into the epoxy resin using mechanical stirring for 10–15 mins. Ultrasonic mixing followed for 30 mins to achieve uniform dispersion, ensuring proper integration of GnPs into the epoxy. As seen in Figure 1(a) and (b), basalt fibers were then impregnated with the GnP/epoxy mixture as they passed through a resin bath maintained at 80°C with an epoxy-to-hardener ratio of 80:20 by weight. The fibers were subsequently wound onto mandrels with a diameter of 72 mm at a winding angle of 55°. After the winding process, the pipes were cured at 120 °C for 3 hrs, followed by post-curing at 140 °C for an additional 3 hrs. The composite pipes were allowed to cool to room temperature before being cut to a length of 50 mm for erosion testing, as shown in Figure 1(c).

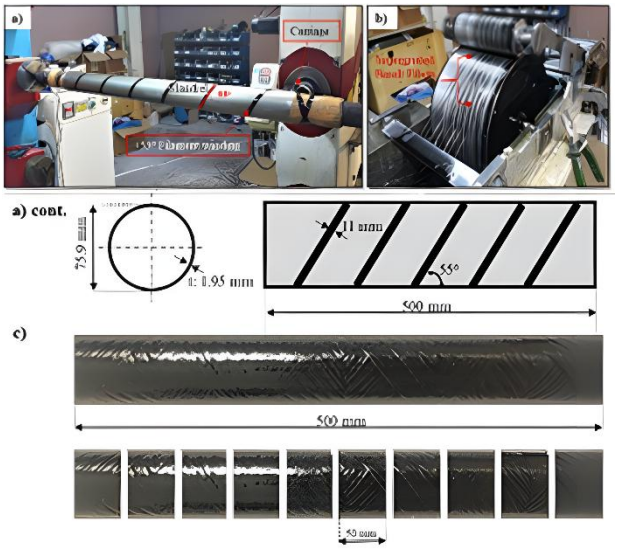

Fig. 1. The filament winding process and dimensions and structure of composite pipes (a), the resin bath and impregnated fibers on the mandrel (b), and erosion test specimens of 50 mm, including an image of the GnP-reinforced composite pipe (c).

2.2 High temperature solid particle erosion test

Solid particle erosion wear tests were conducted on a test rig (Figure 2) designed in accordance with ASTM G211-14 standard [22].

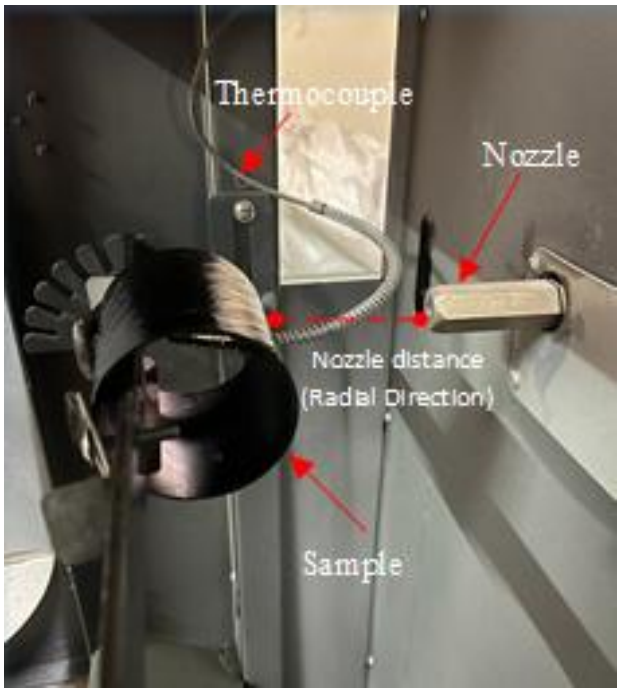

Fig. 2. Placing samples in the testing rig.

Al_2O_3 abrasive powders with a size of ~400 µm were used as erosive particles due to their high temperature resistance Preliminary experiments were carried out to determine the total erosive particle weight and the effects of different erosive weights on two different samples and three different temperatures were analysed. As a result of the preliminary experiments, the erosive particle weight was determined as 200 g to be able to make comparisons between the samples. To see the temperature effect on the samples, the experiments were carried out at room temperature, 50 °C and 100 °C. To keep the temperature stable in the test rig, continuous measurements were made with the help of a thermocouple, and it was ensured that the experiments were carried out at the same temperature in the tests of the test samples. Solid particle erosion tests were performed at three different impingement angles (30°, 60° and 90°). In adjusting the test angle, angle variability was achieved according to the impact in the radial direction by rotating the sample holder to the desired angle as seen in Figure 3. In addition, in this way, an attempt was made to schematic show the eccentricity formation between the nozzle extension and the pipe center depending on the angle change. As a result, the distance between the nozzle and the sample was adjusted to be equal during all experiments in angle changes.

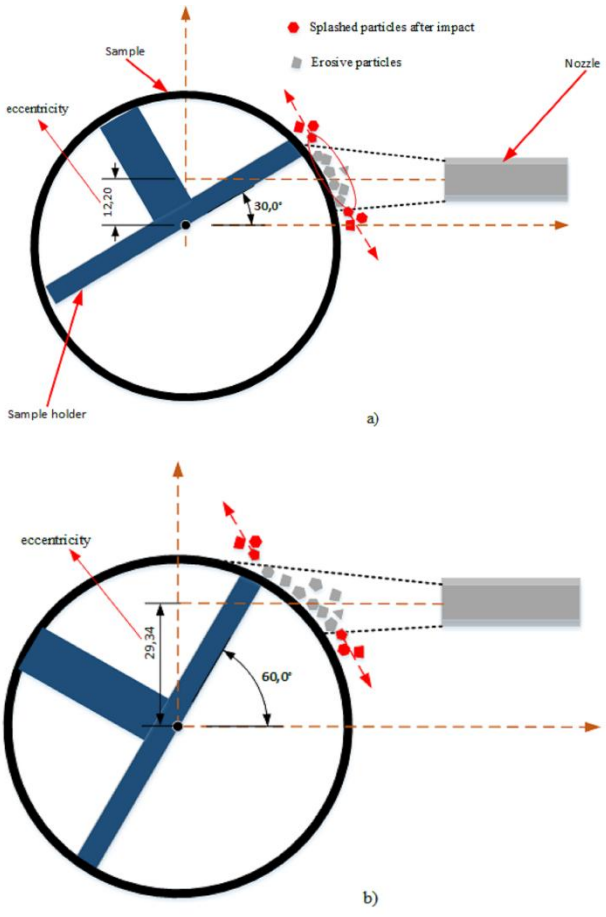

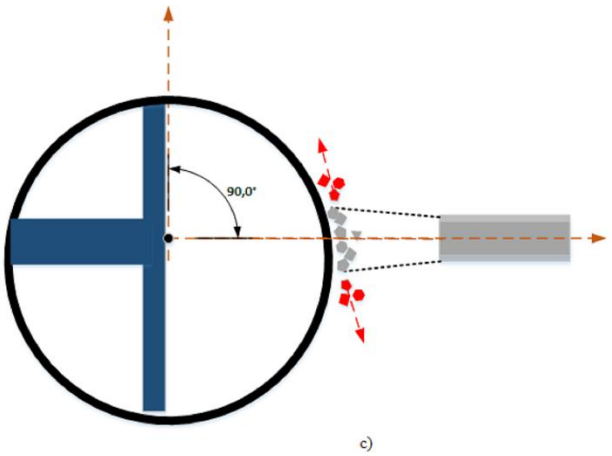

Fig. 3. Schematic view of the erosive particle impingement angle on the samples; a)30°, b)60°, c)90°.

The double disc method, which is an easy and inexpensive method, was used to determine the erosive particle impact velocity. As a result of this method, the impact velocity was determined to be 97 m/s without any perforation in the wall thickness of the sample.

The experiments were carried out under the same conditions with three repetitions due to the possibility of any error.

To see the effects of the erosion rate (ER) of the erodent mass (m) determined by preliminary experiments, sample surface wear conditions were observed and after each test, the weight of the test sample was measured by means of a precision balance with a precision of ±0.1 mg and the outer surface wear conditions of the pipe were examined.

The basic ER formulation is obtained from the ratio of the initial and final sample weights (ΔW) to the erodent mass (m) used.

$$ER = \frac{\text{mass loss of the wearing material } (\Delta W)}{\text{mass of erodent impact the surface } (m)} \quad (1)$$

In determining the erosion rate, as given in the literature [23], the erosion rate (mg/g) value was calculated by using the values of the sample surface hardness value (H), wear coefficient (K), particle velocity (U) and material density (ρ), considering the linear change of erosion, as Hutchings' formula (2):

$$ER = \frac{K\rho U^2}{2H} \quad (2)$$

3. RESULT AND DISCUSSION

3.1. The effect of impingement angle

The graph of the erosion rate depending on the impingement angle caused by the radial impact of erosive particles on the outer surfaces of Basalt pipe (BFRP) and Graphene nanoplates reinforced pipe (GnPs/Basalt pipe) at room temperature is given in Figure 4. The difference between the erosion wear rates of two different pipe materials after the experiments performed under the same conditions proved that the graphene effect, which was included in the literature with this study, has a positive contribution to the erosion resistance. It was concluded that although the impingement angle change depends on the increasing impingement angle in Basalt pipe, the highest erosion rate occurs at 60°–90° impingement angles, which is more dominant at positions where the eccentricity is close to zero, and the impact velocity makes some difference in the process, but compliance with the literature has been revealed [24].

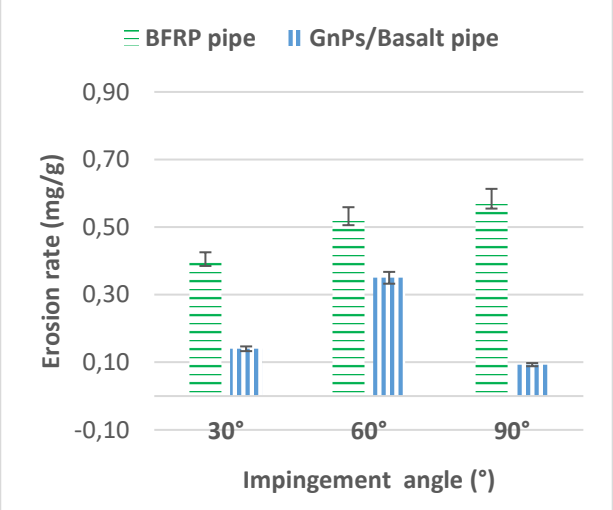

Fig. 4. Erosion rate changes of samples at different impingement angles at room temperature.

At 30° angle, the erosion rate decreased by 20-30% compared to the other impingement angles in Basalt pipe due to the contact variability on the surface. In GnPs/Basalt pipes, the effect of reducing the erosion rate was dominant in all variations of the erosive particle impingement angle. In particular, the erosion rate values for the 60° angle describe the highest erosion in the graphene additive but had an improving effect on the erosion resistance at all impingement angles compared to the Basalt pipe.

The erosive particle exhibited minimum erosion rate at 90° impingement angle, and in pipes with graphene additive, which is a two-dimensional material consisting of carbon atoms with a single atom thickness arranged in a hexagonal honeycomb arrangement, the deformation effect can be explained by the fact that the erosive particles impacting perpendicular to the surface cause less separation from the surface by delaying the crack initiation as a result of graphene forming a durable bond with epoxy on the surface instead of the consecutive crack effect. When the erosive particle impacts at an impingement angle of 30°, the cracking process starts, but the scraper effect is reduced by graphene lubrication compared to the situation in the Basalt pipe and contributed to the increase in erosion resistance.

In addition to room temperature, the experiments were also carried out at 50 °C and 100 °C. Figure 5 shows the erosion rate changes of basalt composite pipes depending on the temperature change. When the graph is analysed, the highest erosion rate occurs at 50 °C and almost the lowest erosion rate occurs when the temperature increases to 100 °C. When the literature studies examining the mechanical properties of polymer composite pipes are examined, it is seen that the stiffness value of these materials decreases with increasing temperature [25]. This can be explained by the fact that the heated erosive particles hitting the outer surface of the pipe when the temperature increases by a limited amount, i.e. 50 °C, break off more particles from the surface or by the thermal embrittlement effect [26]. In addition, the decrease in the storage modulus (E') of the samples in the erosion tests performed at this temperature and the corresponding increase in the loss modulus (E'') can explain the decrease in the erosion rate of the BFRP samples in the erosion tests performed at 100 °C, when the outer surface of the pipe is extremely heated, compared to the tests performed at other temperatures [27-29]. This increase causes the BFRP samples to exhibit viscous behaviour, thereby increasing the mechanical damping capacity (tanδ=E''/E') by dissipating the impact energy more effectively. As a result, the impact energy transferred on impact of erosive particles on the surface is more damped, thus reducing the likelihood of localized damage (cracks and material rupture). This behaviour optimizes crack resistance and energy absorption capacity.

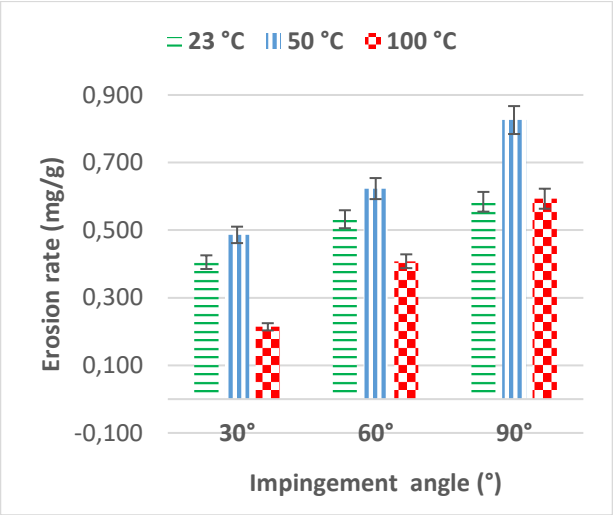

Fig. 5. Graph of erosion rate change with temperature change of basalt pipe.

Graph showing the erosion rates of graphene reinforced composite pipes under the influence of temperature (Figure 6), it is seen that the highest erosion rate is at 50 °C, like that in Basalt pipe.

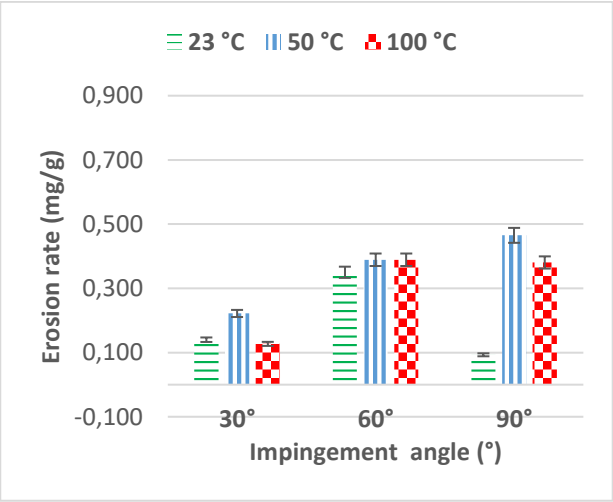

Fig. 6. Graph of erosion rate change with temperature change of GnPs/Basalt pipe.

It was found that the erosion rate of BFRP composites decreased at 100 °C with the addition of graphene. In the literature, the effect of graphene reinforcement on thermal and mechanical properties of epoxy matrix composites has been studied in detail. In particular, the increase in glass transition temperature (Tg), increase in mechanical strength and decrease in coefficient of thermal expansion (CTE) emphasize the positive effects of graphene additive on the matrix [29,30]. As the erosion test temperature increases, BFRP samples begin to soften, and erosive particles

contact the surface of the BFRP composite with increased toughness. This delays the formation of cracks and allows the crack resistance and energy absorption capacity to approach the optimal level. In addition, simulation studies, although less relevant, were also included in the references upon the intensive recommendation of the relevant reviewer who was aware of the originality of our manuscript results [31,32].

3.2. Temperature effect

Solid particle erosion tests of Basalt pipe and GnPs/Basalt pipes at 50 °C are given in Figure 7. As a result of the experiments, it was determined that the erosion resistance of graphene doped pipe was better than Basalt pipe at all impingement angles. This result showed that graphene significantly increased the erosion resistance of Basalt pipe both at room temperature and at other temperatures where the experiments were performed.

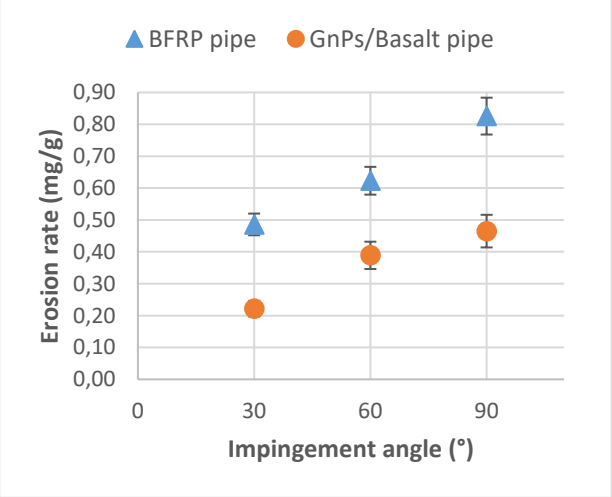

Fig. 7. Erosion rate changes of the samples depending on the impingement angle at 50 °C.

In comparison of 60° and 90° impingement angles of graphene, the adhesion ability between the matrix and graphene was slightly weakened with the increase in temperature compared to room temperature, resulting in a decrease in erosion resistance.

Figure 8 shows the comparative graph of the results of the experiments performed at 100 °C for both Basalt pipe and GnPs/Basalt pipe. Since the increase in temperature reveals the presence of incubation, especially in the presence of graphene, it did not cause a significant difference by suppressing erosion resistance.

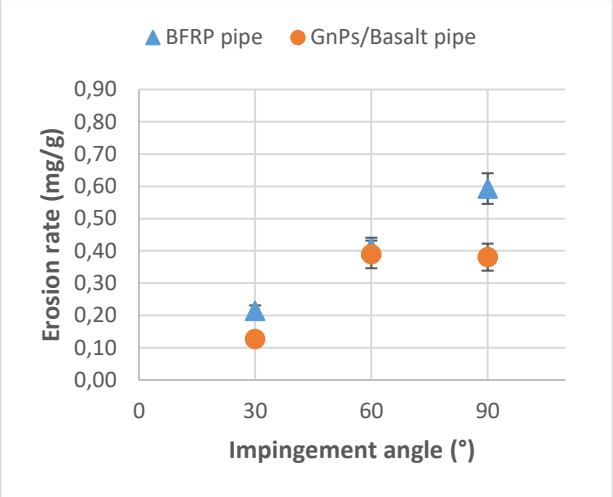

Fig. 8. Erosion rate changes of the samples depending on the impingement angle at 100 °C.

The main situation in this result is interpreted as the presence of temperature in the bond formed between graphene and epoxy affects the significance. In the case of basalt pipe, the primary increase in temperature accelerated the ruptures with the effect of erosive particles between basalt fibers and epoxy, and in the experiments with a temperature of 100 °C, the particle embedding between the matrix and fibers increased effective resistance.

3.3. Erosion damage analyses

Erosion damage of $[\pm 55^{o}]_4$ layered BFRP composite pipes and 0.25% GnPs reinforced BFRP composite pipes produced by filament winding technique were evaluated within the scope of erosion tests performed under different temperature conditions (room temperature, 50°C and 100°C) and impingement angles (30°, 60°, 90°). The obtained macro and scanning electron microscope (SEM) images were examined comparatively to better understand the damage formation mechanisms. SEM analyses were performed at the center and edge regions of the erosion damage and the wear types and damage morphology on the material surface were evaluated in detail.

When the data presented in Figure 9 is examined, it is clearly observed that there are obvious cracks, fragments and irregular erosion marks on the surface in the macro image (a) of the BFRP composite pipe and in the high magnification SEM images (b, c; e, d) of the edge and center regions of the erosion damage.

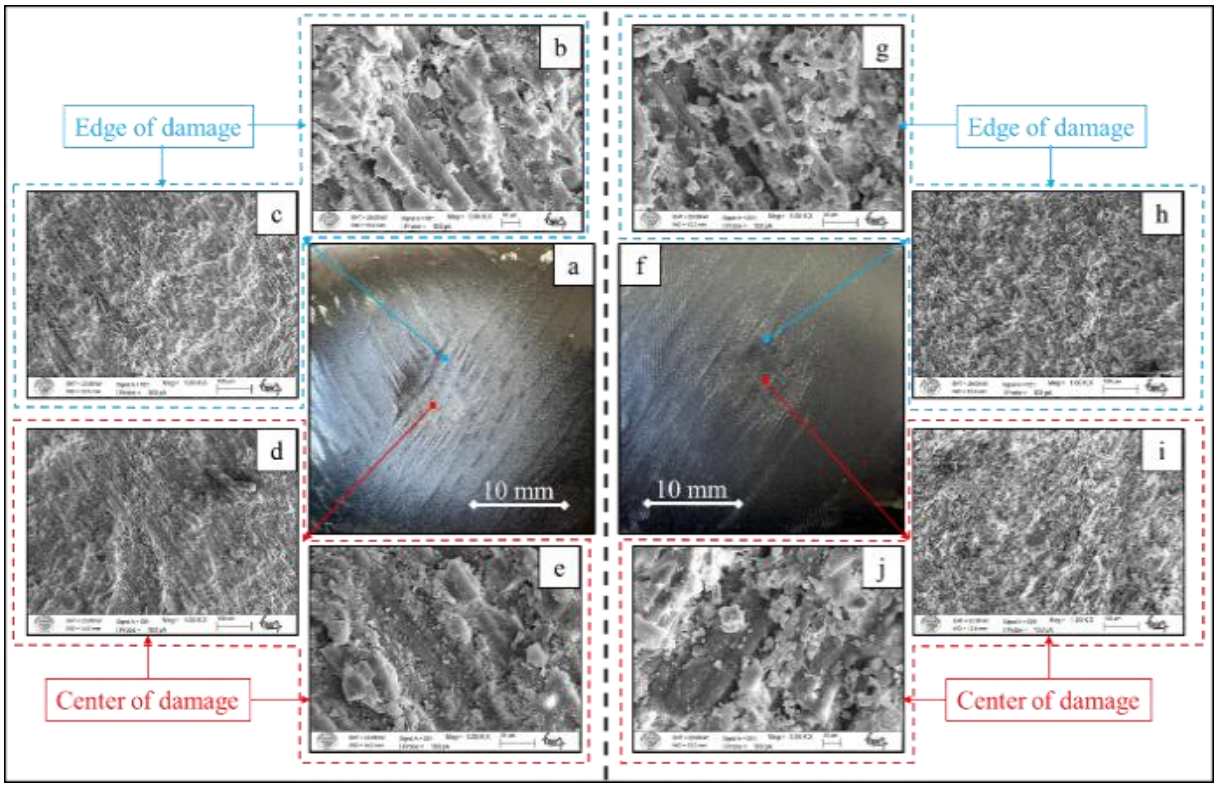

Fig. 9. The erosion damages at 23 °C and 60° impingement angle – Basalt pipe: macro image (a), SEM images of the damage edge; 5000× (b) and 1000× (c), SEM images of the damage center; 5000× (e) and 1000× (d); GnPs/Basalt pipe: macro image (f), SEM images of the damage edge; 5000× (g) and 1000× (h), SEM images of the damage center; 5000× (j) and 1000× (i).

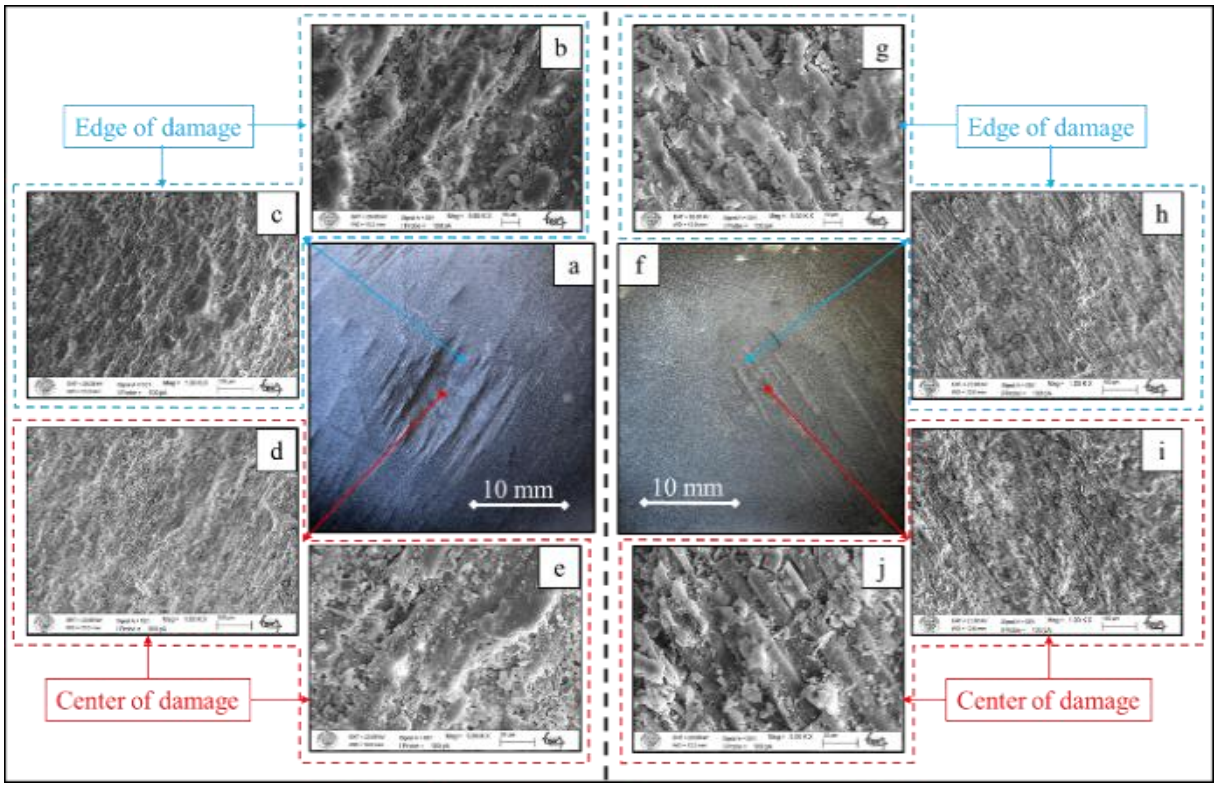

Fig. 10. The erosion damages at 50 °C and 60° impingement angle – Basalt pipe: macro image (a), SEM images of the damage edge; 5000× (b) and 1000× (c), SEM images of the damage center; 5000× (e) and 1000× (d); GnPs/Basalt pipe: macro image (f), SEM images of the damage edge; 5000× (g) and 1000× (h), SEM images of the damage center; 5000× (j) and 1000× (i).

On the other hand, a more homogeneous distribution is detected in the damage region in the macro image (f) and SEM images (g, h; j, i) of the GnPs/Basalt composite pipe. This may indicate that the GnPs reinforcement improves the stress distribution within the material, and the crack propagation progresses indirectly slower.

In addition, it was determined in the SEM analyses that the basalt fibers came to the surface more clearly after erosion, and the fiber appearance was less noticeable in the samples with GnPs reinforcement.

These findings indicate that the GnPs reinforcement delays the formation and propagation of cracks by improving the stress distribution within the material with its mechanical damping effect.

On the other hand, the presence of GnPs reinforcement prevents the emergence of basalt fibers on the damage surface, indicating that it creates a more complete damage morphology.

In Figure 10, an increase in damage intensity is observed in both BFRP and GnPs reinforced composite pipes under an impingement angle of 60° at 50°C.

In the BFRP composite pipe, the thermal stress and possible embrittlement effects caused by the increase in temperature are seen as deeper cracks and rupture zones in the macro image (a) and SEM (b, c; e, d); while in the GnPs/Basalt pipe, the distribution of damage remains relatively more controlled thanks to the lubrication and interfacial bond strengthening effect provided by the GnPs reinforcement.

Figure 11 indicates that the damage intensity decreases in the BFRP composite pipe due to the thermal softening and viscoelastic properties that come into play in the images obtained under an impingement angle of 60° at 100°C.

While it is observed that the cracks are more superficial and the fractures are limited in the SEM images (b, c; e, d), it is thought that the interaction between the epoxy-matrix and GnPs in the GnPs/Basalt composite pipe (f; g, h; j, i) cannot completely suppress the damage in certain cases due to the temperature effect, but the crack initiation is still delayed.

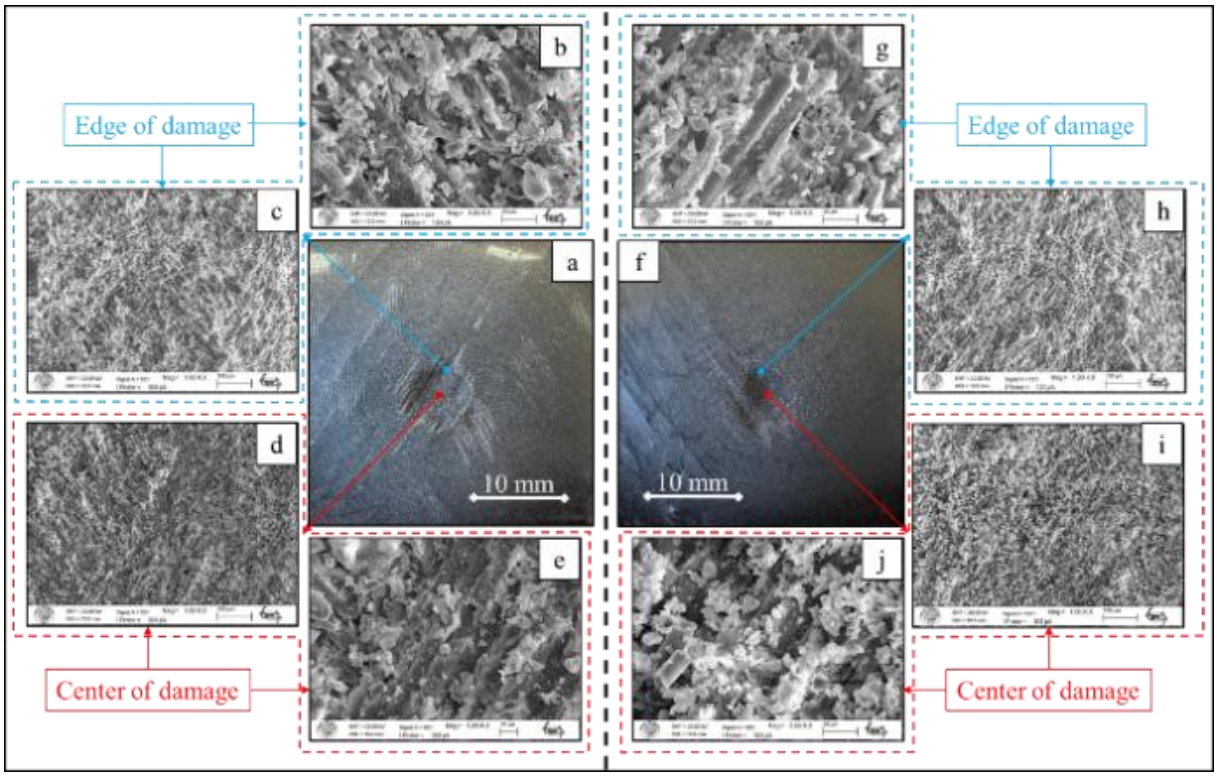

Fig. 11. The erosion damages at 100 °C and 60° impingement angle – Basalt pipe: macro image (a), SEM images of the damage edge; 5000× (b) and 1000× (c), SEM images of the damage center; 5000× (e) and 1000× (d); GnPs/Basalt pipe: macro image (f), SEM images of the damage edge; 5000× (g) and 1000× (h), SEM images of the damage center; 5000× (j) and 1000× (i).

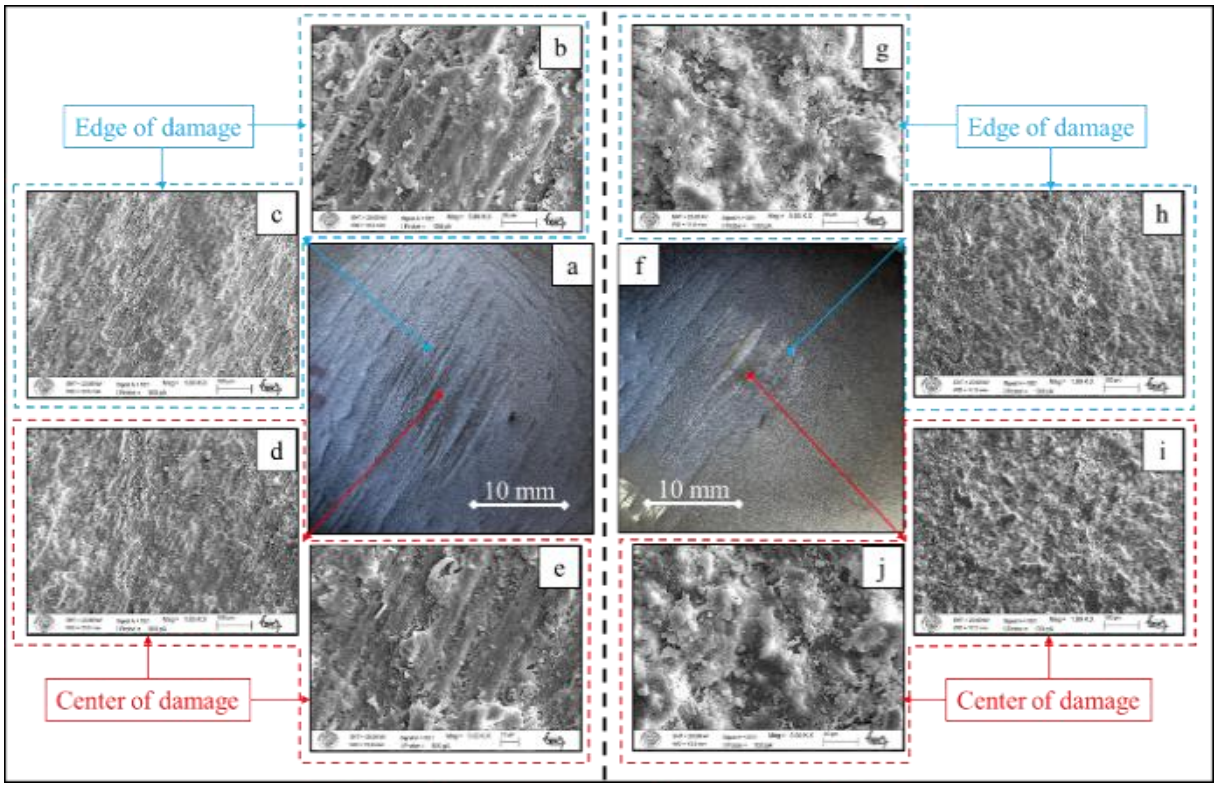

Fig. 12. The erosion damages at 50 °C and 30° impingement angle – Basalt pipe: macro image (a), SEM images of the damage edge; 5000× (b) and 1000× (c), SEM images of the damage center; 5000× (e) and 1000× (d); GnPs/Basalt pipe: macro image (f), SEM images of the damage edge; 5000× (g) and 1000× (h), SEM images of the damage center; 5000× (j) and 1000× (i).

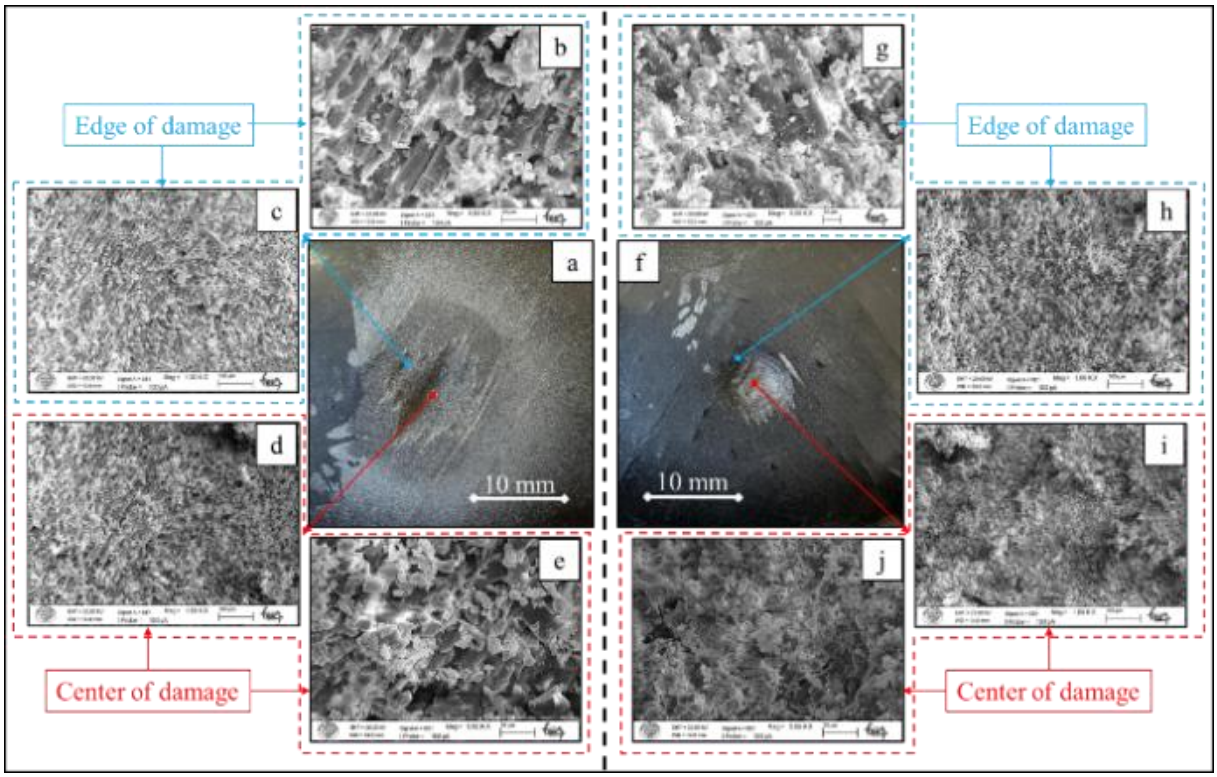

Fig. 13. The erosion damages at 100 °C and 90° impingement angle – Basalt pipe: macro image (a), SEM images of the damage edge; 5000× (b) and 1000× (c), SEM images of the damage center; 5000× (e) and 1000× (d); GnPs/Basalt pipe: macro image (f), SEM images of the damage edge; 5000× (g) and 1000× (h), SEM images of the damage center; 5000× (j) and 1000× (i).

When the images of Basalt pipe and GnPs/Basalt pipe obtained at 50°C and 30° impingement angle are examined in Figure 12, it is observed that although the lower impingement angle increases the scraping effect of the particles, the erosion rates are lower for both test samples compared to the tests at 50°C and 60° impingement angle due to the decrease in the erosive particle area in contact with the surface due to the effect of the pipe geometry.

In addition, the macro and SEM images presented in Figure 10 and Figure 12 reveal a significant decrease in damage severity.

While minimal and local scraping marks are evident in the Basalt pipe samples in Figure 10 (macro: a, f; SEM: b, c; e, d), the damage pattern is more homogeneous and less aggressive in the GnPs reinforced pipes (SEM: g, h; j, i). These findings indicate that GnPs reinforcement positively affects the material behavior and reduces the severity of erosion-induced surface damage.

In Figure 13, under the vertical impingement angle of 90° at 100°C, serious damages occur in the BFRP composite pipe because of intense, mechanical repetitive impacts created by full vertical contact, while the damage intensity is relatively reduced in the GnPs/Basalt composite pipe thanks to the resistance provided by the GnPs reinforcement. In addition, the 90° impingement angle at 100°C increases the erosion rate of the BFRP composite pipe by approximately 50% compared to the 60° impingement angle, while this effect is much milder in the GnPs reinforced composite pipes.

In the macro image comparisons (Figure 11a and Figure 13f), it is observed that the Basalt pipe creates distinct and deep damage traces under the 90° impact conditions, while the damage pattern in the GnPs reinforced samples is similar for both angles, indicating that GnPs keeps the severity of the damage under control by improving the energy absorption and stress distribution within the material.

In Figure 14, the erosion damages of the BFRP composite pipe under the 30° impingement angle at 50°C and 100°C conditions were examined. In the macro images (100°C: a; 50°C: f), a significant decrease in damage intensity was observed due to the increase in temperature.

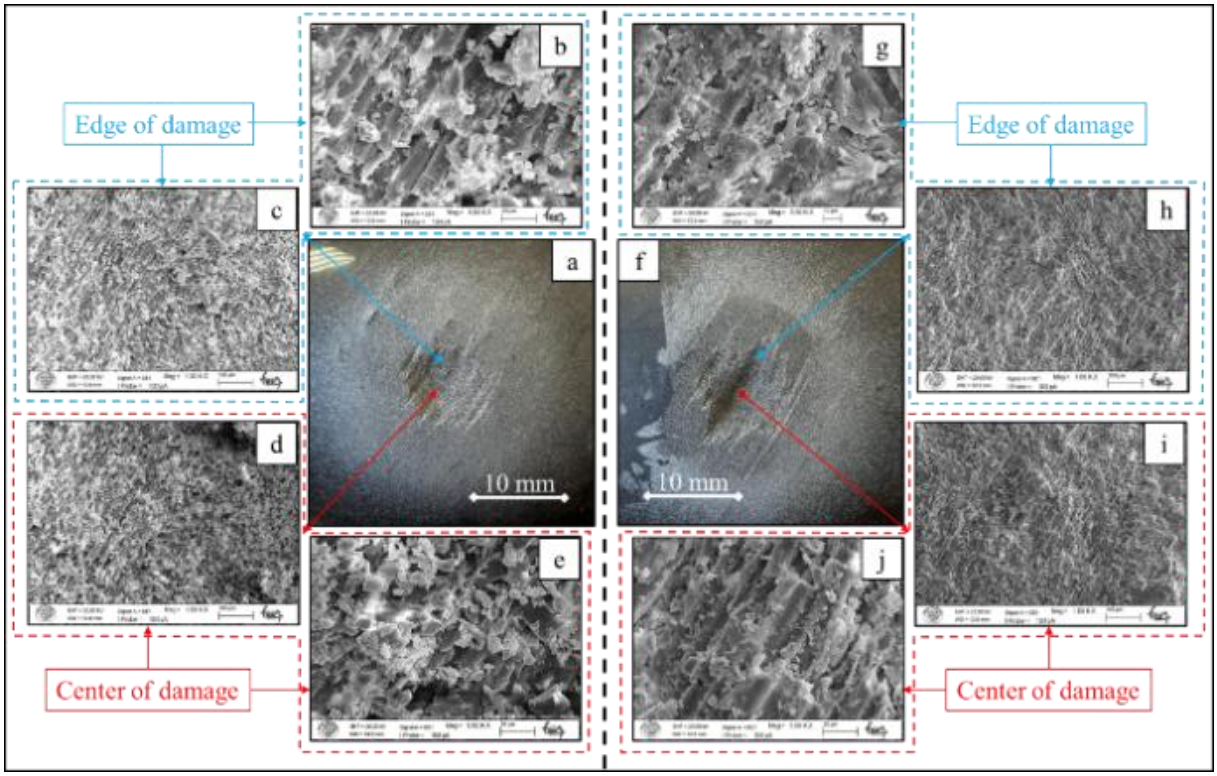

Fig. 14. The erosion damages of Basalt pipe at 30° impingement angle – at 100 °C: macro image (a), SEM images of the damage edge; 5000× (b) and 1000× (c), SEM images of the damage center; 5000× (e) and 1000× (d); at 50 °C: macro image (f), SEM images of the damage edge; 5000× (g) and 1000× (h), SEM images of the damage center; 5000× (j) and 1000× (i).

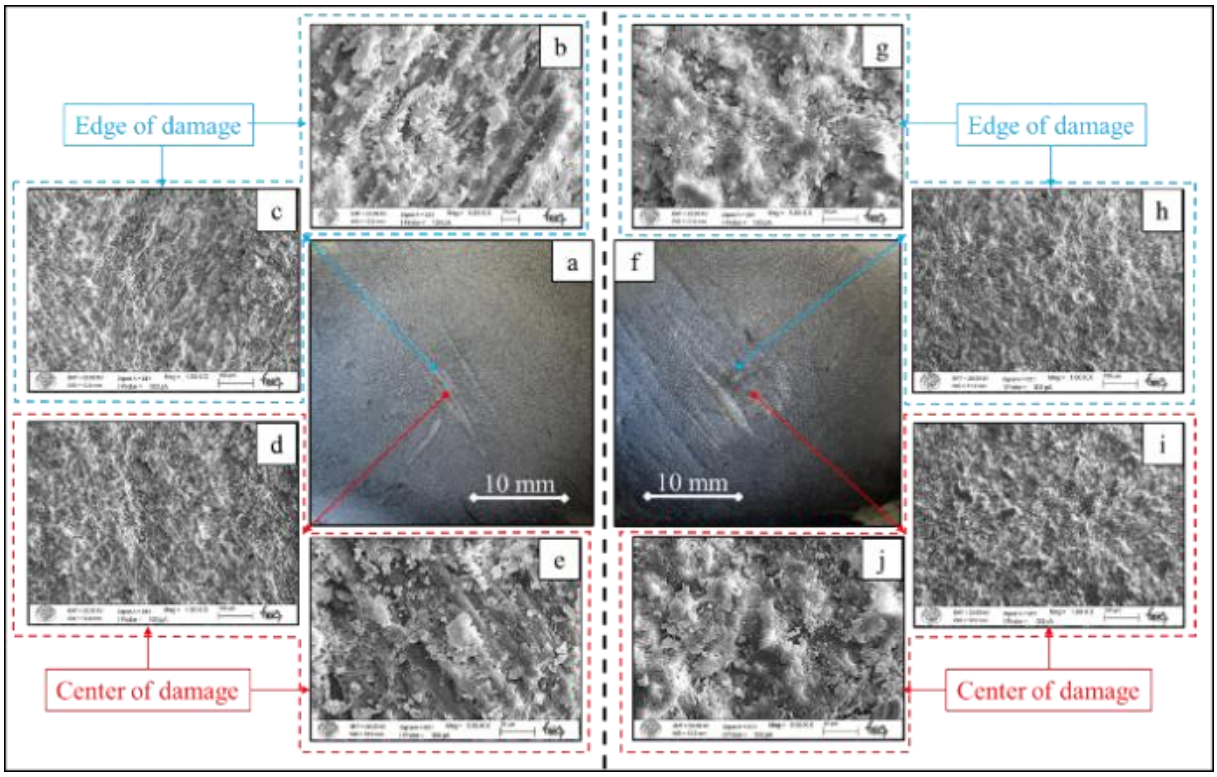

Fig. 15. The erosion damages of GnPs/Basalt pipe at 30° impingement angle – at 100 °C: macro image (a), SEM images of the damage edge; 5000× (b) and 1000× (c), SEM images of the damage center; 5000× (e) and 1000× (d); at 50 °C: macro image (f), SEM images of the damage edge; 5000× (g) and 1000× (h), SEM images of the damage center; 5000× (j) and 1000× (i).

This situation is also supported by the thermal softening of the matrix and the activation of viscoelastic properties under high temperature. In the SEM images (edge and center regions; 100°C: b, c, e, d; 50°C: g, h, j, i), it is seen that the 100°C condition limits the erosion damage in a more controlled manner, while the damage at 50°C creates more distinct and sharp scratches.

In Figure 15, erosion damages of GnPs/Basalt composite pipe under 30° impingement angle at 50°C and 100°C conditions are discussed. In macro images (100°C: a; 50°C: f), it is determined that increasing the temperature significantly reduces the erosion damage. In SEM analyses (edge and center regions; 100°C: b, c, e, d; 50°C: g, h, j, i), it is observed that the damage intensity is lower than that of BFRP composite pipe at both 50°C and 100°C due to the mechanical damping effect provided by GnPs reinforcement and the damage pattern is more homogeneously distributed.

In both pipe types, when the temperature increases from 50°C to 100°C, the erosion rate and damage severity decrease. In BFRP composite pipe, thermal softening and viscoelastic properties brought by high temperature contribute to the reduction of damage intensity. In addition, in GnPs reinforced composite pipes, the mechanical damping and energy absorption effect of GnPs further reduces erosion damage under both temperature conditions, resulting in lower damage rates compared to Basalt pipe.

These findings are clearly observed in macro image comparisons (Figures 14a and 14f; Figures 15a and 15f). In conclusion, this comprehensive damage analysis reveals that GnPs reinforcement can significantly reduce erosion damage under different temperature and impingement angle conditions, especially by delaying crack initiation and increasing mechanical damping capacity.

4. CONCLUSION

To focus on experimental specificity, two types of experimental samples were produced using the filament winding technique, specifically focusing on [±55º], layered, undoped composite tubes and 0.25 wt% GnPs-reinforced composite tubes. The presence of graphene

reinforcement was specifically investigated in the experiments, and detailed comparisons at three different temperatures and three different angles revealed positive contributions to erosion resistance. Furthermore, it was concluded that the present results are due to the presence of nanoplates on the sample surfaces, which act as lubricants and strengthen interfacial bonds.

In the tests of basalt pipes at different temperatures, the highest erosion rate was observed at 50 °C. In addition, when the impingement angle effect on the basalt pipe is considered, the highest erosion rate occurred at 90° erosive angle. The wear images at this angle value showed distinct and deep damage marks. When the erosion images of the basalt pipe obtained under 30° impingement angles were analysed, although the lower impingement angle increased the scraper effect of the particles, the lowest erosion rate was obtained at this angle at all temperature values as a result of the decrease in the erosive particle area in contact with the surface due to the effect of the pipe geometry. When the erosion rate changes of GnPs/Basalt pipes at different temperatures are examined, the highest erosion rate was at 50 °C, like basalt pipes. However, when the erosive particle angle variability was examined, the 60° impingement angle was the angle at which the erosion resistance was the least. In addition, the graphene effect caused an increase in erosion resistance by approximately 1.5 times in experiments performed at high temperatures.

From the SEM images taken after the wear of the samples after the experiments performed at room temperature, it was concluded that GnPs reinforcement prevents stress concentration with mechanical damping effect and slows down crack propagation.

Experiments at 100 °C has been observed the presence of incubation period because of the thermal softening and viscoelastic properties of the matrix under high temperature to increase the erosion resistance. As a result of the erosion tests carried out under different temperature and angle conditions, it was concluded that GnPs reinforcement can significantly reduce erosion damage, especially due to its ability to delay crack initiation and increase mechanical damping capacity.

REFERENCES

[1] Y. Chen and C. Zhang, "Stability analysis of pultruded basalt fiber-reinforced polymer (BFRP) tube under axial compression," *Composite Structures*, vol. 327, p. 117660, Oct. 2023, doi: 10.1016/j.compstruct.2023.117660.

[2] A. A. J. Kumar, N. P. A. Ramaseshan, and T. Lakshmanan, "Tribological Analysis on Basalt/Aramid Hybrid Fiber Reinforced Polyimide Composites: an alternate brake pad material," *Tribology in Industry*, vol. 43, no. 2, pp. 334–347, Jun. 2021, doi: 10.24874/ti.912.06.20.12.

[3] P. Jagadeesh, S. M. Rangappa, and S. Siengchin, "Basalt fibers: An environmentally acceptable and sustainable green material for polymer composites," *Construction and Building Materials*, vol. 436, p. 136834, Jun. 2024, doi: 10.1016/j.conbuildmat.2024.136834.

[4] S. M. Darshan, B. Suresha, and I. M. Jamadar, "Optimization of Abrasive Wear Parameters of Halloysite Nanotubes Reinforced Silk/Basalt Hybrid Epoxy Composites using Taguchi Approach," *Tribology in Industry*, vol. 44, no. 1, pp. 253–267, Jun. 2022, doi: 10.24874/ti.1131.06.21.08.

[5] K. V. Balaji, K. Shirvanimoghaddam, and M. Naebe, "Multifunctional basalt fiber polymer composites enabled by carbon nanotubes and graphene," *Composites Part B Engineering*, vol. 268, p. 111070, Oct. 2023, doi: 10.1016/j.compositesb.2023.111070.

[6] K. Y. E. Awwad, "Effects of Adding Graphite to Epoxy Resin on its Mechanical Properties and Mild-to-Severe Wear Performance at its Heat Distortion Temperature," *Tribology in Industry*, vol. 46, no. 2, pp. 298–314, Jun. 2024, doi: 10.24874/ti.1552.09.23.01.

[7] U. R. Hashim, A. Jumahat, and M. Jawaid, "Mechanical properties of hybrid graphene Nanoplatelet-Nanosilica filled unidirectional basalt fibre composites," *Nanomaterials*, vol. 11, no. 6, p. 1468, Jun. 2021, doi: 10.3390/nano11061468.

[8] A. Shivamurthy, R. Boranna, R. K. Jagannat, G. R. Prashanth, S. Bheemappa, and S. M. Darshan, "Mechanical properties and analysis of two-body abrasive wear behaviour of graphene modified Carbon/Epoxy composites using Taguchi's technique," *Tribology in Industry*, vol. 46, no. 1, pp. 66–79, Mar. 2024, doi: 10.24874/ti.1512.07.23.09.

[9] H. S. Kim, H. S. Bae, J. Yu, and S. Y. Kim, "Thermal conductivity of polymer composites with the geometrical characteristics of graphene nanoplatelets," *Scientific Reports*, vol. 6, no. 1, May 2016, doi: 10.1038/srep26825.

[10] Y. Şahin and D. B. Patrick, "Effects of nano-Al2O3 and PTFE fillers on tribological property of basalt fabric-reinforced epoxy composites," *Tribology - Materials Surfaces & Interfaces*, vol. 15, no. 4, pp. 258–277, Oct. 2021, doi: 10.1080/17515831.2020.1854509.

[11] K. Yee and M. H. Ghayesh, "A review on the mechanics of graphene nanoplatelets reinforced structures," *International Journal of Engineering Science*, vol. 186, p. 103831, Feb. 2023, doi: 10.1016/j.ijengsci.2023.103831.

[12] M. Bagci, "Determination of solid particle erosion with Taguchi optimization approach of hybrid composite systems," *Tribology International*, vol. 94, pp. 336–345, Sep. 2015, doi: 10.1016/j.triboint.2015.09.032.

[13] M. Kishore, M. Amrita, and B. Kamesh, "Tribological properties of basalt-jute hybrid composite with graphene as nanofiller," *Materials Today Proceedings*, vol. 43, pp. 244–249, Jan. 2021, doi: 10.1016/j.matpr.2020.11.654.

[14] M. Dheepthi, T. Sivagangai, P. M. Radhakrishnan, and R. Santhanakrishnan, "Effect of milled glass fiber on fatigue life of basalt fiber reinforced composites," *Materials Today Proceedings*, Jan. 2023, doi: 10.1016/j.matpr.2023.01.228.

[15] L. Wu *et al.*, "Wear resistance of graphene nano-platelets (GNPs) reinforced AlSi10Mg matrix composite prepared by SLM," *Applied Surface Science*, vol. 503, p. 144156, Oct. 2019, doi: 10.1016/j.apsusc.2019.144156.

[16] M. H. Islam, S. Afroj, M. A. Uddin, D. V. Andreeva, K. S. Novoselov, and N. Karim, "Graphene and CNT-Based Smart Fiber-Reinforced Composites: A review," *Advanced Functional Materials*, vol. 32, no. 40, Aug. 2022, doi: 10.1002/adfm.202205723.

[17] H. Sepetcioglu, S. M. Demet, and M. Bagci, "A comprehensive experimental study of enhanced solid particle erosive resistance on the inner/outer surface of graphene nanoplatelets modified basalt/epoxy composite pipe," *Polymer Composites*, vol. 44, no. 10, pp. 6944–6956, Aug. 2023, doi: 10.1002/pc.27609.

[18] S. R. More, D. V. Bhatt, and J. V. Menghani, "Study of the Parametric Performance of Solid Particle Erosion Wear under the Slurry Pot Test Rig," *Tribology in Industry*, vol. 39, no. 4, pp. 471–481, Dec. 2017, doi: 10.24874/ti.2017.39.04.06.

[19] S. Zhou *et al.*, "Facile preparation of multiscale graphene-basalt fiber reinforcements and their enhanced mechanical and tribological properties for polyamide 6 composites," *Materials Chemistry and Physics*, vol. 217, pp. 315–322, Jun. 2018, doi: 10.1016/j.matchemphys.2018.06.080.

[20] Q.-H. Wang, X.-R. Zhang, and X.-Q. Pei, "Study on the friction and wear behavior of basalt fabric composites filled with graphite and nano-SiO2," *Materials & Design (1980-2015)*, vol. 31, no. 3, pp. 1403–1409, Sep. 2009, doi: 10.1016/j.matdes.2009.08.041.

[21] A. R. Al-Obaidi, J. Alhamid, and H. Khalaf, "Unsteady behaviour and plane blade angle configurations' effects on pressure fluctuations and internal flow analysis in axial flow pumps," *Alexandria Engineering Journal*, vol. 99, pp. 83–107, May 2024, doi: 10.1016/j.aej.2024.04.048.

[22] M. Demirci and M. Bagci, "Alternative system design for high temperature solid particle erosion wear problem," *Tribology Letters*, vol. 69, no. 1, Jan. 2021, doi: 10.1007/s11249-021-01400-6.

[23] I. Hutchings and P. Shipway, *Tribology: Friction and Wear of Engineering Materials*. Butterworth-Heinemann. 2017

[24] S. M. Demet, H. Sepetcioglu, and M. Bagci, "Solid particle erosion behavior on the outer surface of Basalt/Epoxy composite pipes produced by the filament winding technique," *Polymers*, vol. 15, no. 2, p. 319, Jan. 2023, doi: 10.3390/polym15020319.

[25] H. Benyahia, M. Tarfaoui, A. E. Moumen, D. Ouinas, and O. H. Hassoon, "Mechanical properties of offshoring polymer composite pipes at various temperatures," *Composites Part B Engineering*, vol. 152, pp. 231–240, Jul. 2018, doi: 10.1016/j.compositesb.2018.07.014.

[26] H. U. Khalid, M. C. Ismail, and N. Nosbi, "Permeation Damage of polymer liner in oil and gas pipelines: a review," *Polymers*, vol. 12, no. 10, p. 2307, Oct. 2020, doi: 10.3390/polym12102307.

[27] N. Saba, M. Jawaid, O. Y. Alothman, and M. T. Paridah, "A review on dynamic mechanical properties of natural fibre reinforced polymer composites," *Construction and Building Materials*, vol. 106, pp. 149–159, Dec. 2015, doi: 10.1016/j.conbuildmat.2015.12.075.

[28] V. Mahesh, "Enhancing abrasion resistance in Jute/Epoxy composites: The role of silicon carbide fillers in wear prevention," *Tribology in Industry*, vol. 47, no. 7, pp. 1–11, Mar. 2025, doi: 10.24874/ti.1733.08.24.11.

[29] S.-C. Shiu and J.-L. Tsai, "Characterizing thermal and mechanical properties of graphene/epoxy nanocomposites," *Composites Part B Engineering*, vol. 56, pp. 691–697, Sep. 2013, doi: 10.1016/j.compositesb.2013.09.007.

[30] H. Ribeiro *et al.*, "Glass transition improvement in epoxy/graphene composites," *Journal of Materials Science*, vol. 48, no. 22, pp. 7883–7892, Aug. 2013, doi: 10.1007/s10853-013-7478-3.

[31] A. R. Al-Obaidi and J. Alhamid, "Experimental and simulation analyses of the hydraulic complex internal flow characteristics in an axial pump based on varying frequency vibration ranges technique," *International Journal on Interactive Design and Manufacturing (IJIDeM)*, vol. 19, no. 5, pp. 3661–3681, Aug. 2024, doi: 10.1007/s12008-024-02012-9.

[32] A. R. Al-Obaidi and J. Alhamid, "Analysis of unsteady internal flow characteristics in axial pump with varying number of blades using computational modelling and vibration techniques," *Flow Measurement and Instrumentation*, vol. 99, p. 102654, Jul. 2024, doi: 10.1016/j.flowmeasinst.2024.102654.